Biomaterials 206 (2019) 61–72

Contents lists available at ScienceDirect

Biomaterials

journal homepage: www.elsevier.com/locate/biomaterials

Original Research Article

Nitrogen-doped graphene quantum dots (N-GQDs) perturb redox-sensitive system *via* the selective inhibition of antioxidant enzyme activities in zebrafish

Shun Deng[a,b,1], Ailing Fu[b,1], Muhammad Junaid[a,c], Yan Wang[a,c], Qian Yin[a], Chen Fu[b], Li Liu[a,c], Dong-Sheng Su[a], Wan-Ping Bian[a,c], De-Sheng Pei[a,c,*]

[a] Key Laboratory of Reservoir Aquatic Environment, Chongqing Institute of Green and Intelligent Technology, Chinese Academy of Sciences, Chongqing 400714, China
[b] College of Pharmaceutical Sciences, Southwest University, Chongqing 400715, China
[c] University of Chinese Academy of Sciences, Beijing 100049, China

ARTICLE INFO

Keywords:
Danio rerio
N-GQDs
Redox system
Antioxidant enzyme activity
USGO

ABSTRACT

Graphene quantum dots (GQDs) are well-known for its potential applications for bioimaging, biosensor, and drug carrier in biomedicine. GQDs are well characteristic of intrinsic peroxidase-like catalytic activity, which is proven effective in scavenging the free radicals, such assuperoxide anion, hydrogen peroxide, and hydroxyl radical. GQDs are also well praised for its low *in vivo* and *in vitro* toxicity. Here, we found that nitrogen-doped GQDs (N-GQDs) can strongly disturb redox-sensitive system *via* the selective inhibition of endogenous antioxidant enzyme activities in zebrafish. The enzyme activities or transcription levels of a battery of hemoproteins including catalase (CAT), superoxide dismutase (SOD), respiratory chain complex I, complex III, hemoglobin (Hb), and myeloperoxidase (MPO), were significantly suppressed by N-GQDs. We also found that N-GQDs activated the cytochrome P450 monooxygenase (*e.g. cyp1a*) and the associated aryl-hydrocarbon receptor repressors (*ahrr1* and *ahrr2*) in zebrafish embryos. Compared to the ultrasmall graphene oxide (USGO), N-GQDs exhibited stronger fluorescent permeability and tissue-specific bio-accumulative effects. Taken together, our findings highlighted that exposure to N-GQDs can disrupt endogenous antioxidant enzyme activities, possibly *via* the competitive inhibition of electron transfer process. Our results in this study provided solid data for biosafety evaluations of various types of GQDs, and created an alert for the future biomedical applications of N-GQDs.

1. Introduction

Graphene quantum dots (GQDs) are structurally composed of single-layer or multiple layers of graphene (G), for sizes typically below 20 nm, which are considered as quasi-zero-dimensional nanomaterials [1]. GQDs inherit many structural attributes from G and exhibit the desirable electro-optic properties of quantum dots (QDs), such as the strong photoluminescence (PL), highly tunable band gaps, excellent photostability, which are superior to other semiconductor quantum dots (SQDs) and carbon quantum dots (CQDs) [2,3]. Previous studies highlighted the use of GQDs-encapsulated probes for highly sensitive cellular and tissue-specific imaging. Some pioneering studies also showed that GQDs can reduce the viability of cancer cells and bacteria by using its intrinsic property of catalase-like activities [4]. Thus, GQDs are the promising fluorophores in replacement of toxic organic dyes in bioimaging and optical sensing, and the potential enhancers in the treatment of cancer and other diseases in pharmaceutics and theranostics [5].

Generally, GQDs are fabricated through the conventional 'top-down' and 'bottom-up' methods; the former is a direct splitting way to produce small size nanoparticles through the acid-assisted cutting of different carbon sources. However, for the top-down method, the quantum yields (QYs) are usually lower than 1%. In contrast, the 'bottom-up' methods are organic synthesis using carbohydrate sources (*e.g.* citric acid, glucose), generating relatively large nanodots with occasional high polydispersity [6]. QYs of GQDs can be greatly improved by surface modification of GQDs in terms of surface passivation and heteroatom doping [1], and there have been reports about the high QYs of surface-modified

* Corresponding author. Key Laboratory of Reservoir Aquatic Environment, Chongqing Institute of Green and Intelligent Technology, Chinese Academy of Sciences, Chongqing 400714, China.
E-mail addresses: peids@cigit.ac.cn, deshengpei@gmail.com (D.-S. Pei).
[1] These authors contributed equally to this work.

https://doi.org/10.1016/j.biomaterials.2019.03.028
Received 15 September 2018; Received in revised form 3 March 2019; Accepted 19 March 2019
Available online 23 March 2019
0142-9612/

GQDs [7–9]. However, surface engineering can change the oxidation states of pristine GQDs that lead to specific spectrum-shifting and varying PL intensity. Our previous study revealed that more than 20% QYs of nitrogen-doped reduced GQDs (N-GQDs) are quantified according to an improved solvothermal synthesis [10].

Besides the prosperous application of GQDs in biocomposites, it remains controversial whether GQDs exert adverse effects on living organisms, owing to its inherent G-like properties. During the past decade, the nanotoxicity of G and associated nanomaterials, such as carbon nanotubes (CNTs) and graphene oxide (GO), have been extensively investigated. In general, the over-production of reactive oxygen species (ROS) has been observed as the major cause of oxidative stress and apoptosis from *in vitro* to *in vivo* models. Some key molecular signals, such as Toll-like receptor 4 [11], JNK-1 [12], IgG [13], and Integrins [14], were identified to be significantly triggered by CNTs and GO, and most of these activators were closely related to ROS-induced signaling pathways. Current knowledge about the low toxicity of GQDs was mainly acquired from *in vitro* toxicity assays and few *in vivo* toxicity evaluations [15–22]. Moreover, it remains an outstanding question of whether the signaling pathways activated by CNTs or GO are selectively recruited by GQDs-induced apoptosis. Therefore, to clarify the potential health risks of GQDs, the molecular *in vivo* toxicity of GQDs is of great importance.

Mouse (*Mus musculus*) and zebrafish (*Danio rerio*) are common animal models for nanotoxicity assessment. Mouse models are usually confronted with high cost, time-consuming, and sampling constraints. In contrast, zebrafish possess many virtues, including the small body, optical-transparency, high fecundity, and low husbandry cost [23]. Due to the conserved evolutionary modules in the zebrafish genome, zebrafish hold the developmental profile that is generally comparable to that in humans. Specifically, the transparent cardiovascular system at the early stage enables them to be observed conveniently, compared to other model systems [24,25]. Previously, zebrafish have been widely used for the toxicity evaluation of a series of nanomaterials, including CNTs [26], carbon graphene oxide (GO) [27,28], semiconductor QDs [29–32]. However, there are few studies about the toxicity assessment of GQDs on zebrafish development [33].

In this study, an integrative analysis was performed combing the quantification of reactive oxygen species (ROS), *in vitro* and *in vivo* bioassays for various antioxidant enzymes, and *in vivo* detection of apoptosis in zebrafish embryos after exposure to N-GQDs and USGO. Further, the molecular markers related to antioxidant enzymes were investigated using qPCR, whole-mount *in situ* hybridization (ISH), and western blotting (WB). Our study aimed to broaden the knowledge of *in vivo* nanotoxicological effects of N-GQDs and other nanoparticles (NPs) and associated signaling pathways, thereby providing data for the risk-assessment model system of NPs nanotoxicity. Moreover, this study pioneered the basic knowledge for the potential use of GQDs in biomedical fields.

2. Methods

2.1. Ethics statement

All zebrafish experiments were performed according to the Guiding Principles for the Care and Use of Laboratory Animals, and were approved by the Animal Care Committee of Chongqing Institute of Green and Intelligent Technology, Chinese Academy of Sciences (Approval ID: ZKCQY0218).

2.2. Chemicals and reagents

Chemicals used for NPs fabrication and other bioassays in this study are listed as follows: graphene oxide powder (XFNANO Materials Tech Co., Ltd. Nanjing, China), *N*, *N*-Dimethylformamide (Sigma Aldrich), FITC-BSA (Bioss Inc., Beijing, China), 2′, 7′-Dichlorodihydrofluorescein (D6883, Sigma Aldrich), hydrogen peroxide (Chengdu Kelong Chemical Company), catalase (C1345, Sigma Aldrich), *o*-dianisidine (D9143, Sigma-Aldrich), acridine orange (AO, Sigma-Aldrich), ethidium bromide (EB, Sigma-Aldrich), methane-sulfonate salt (MS-222, 98%, Aladdin), phosphate buffer solution (1 × PBS, pH 7.4, Gibco), dulbecco's modified eagle medium (DMEM, Gibco).

2.3. Nanoparticles (NPs) preparation

The as-prepared N-GQDs for toxicity assessment were synthesized according to our laboratory's method [10]. The final N-GQDs solutions were condensed at a concentration of 4 mg/mL. Ultrasmall graphene oxide (USGO) prepared for toxicity assays was fabricated according to Zhang's method [34], and the end-product was diluted to 2 mg/mL stock solution with E3 embryo culture medium [28]. To monitor the bio-distribution of USGO in zebrafish, we performed chemical coupling by modifying USGO with FITC according to the previous method [35].

2.4. Surface characterization

Nano-surface properties of N-GQDs and USGO were imaged by atomic force microscope (Dimension FastScan, Bruker Corporation, Germany). NPs samples for AFM were prepared in water dispersion and distributed uniformly on mica substrates (Zhongjingkeyi Technology Co., Ltd, Beijing, China), and then naturally dried in a clean container before testing. By loading the same NPs solutions onto an electron microscopy copper grid (300 mesh size), nanostructures of N-GQDs and USGO were determined with a Tecnai G2 20 Transmission Electron Microscope (TEM) (FEI Co.), and nanoscale feature sizes were measured and calculated with Nanomeasure software. The statistical number of nanoparticles was less than 100. X-ray photoelectron spectroscopy (XPS) spectra were acquired with a Kratos Axis UltraDLD spectrometer (Kratos, Manchester, England) using a monochromatic Al Ka source at 1486.6 eV. Agilent Cary 630 FTIR Spectrometer was also used to compare the functional commonality between USGO and its progenitor (GO). The surface charge of two nanoparticles in different mediums was measured using a Zetasizer Nano ZS apparatus (Malvern Instruments Ltd, Malvern, U.K.).

2.5. Zebrafish husbandry and NPs exposure

Zebrafish strains including wide-type AB and *Tg* (*fli:eGFP*) were raised at constant temperature (28 °C) and photoperiod (14: 10 LD), and fed three times daily with the newly-hatched brine shrimp (*Artemia nauplii*). Zebrafish at about 4 months old were maintained for spawning, and the newly-laid eggs for NPs exposure were collected at 4 h post fertilization (hpf). Fifty well-developed embryos were picked out and transferred into each well of six-well plates by supplementing with various concentrations of NPs solutions (0, 25, 50, and 100 μg/mL), and each concentration group was treated in triplicate. Developmental indices, such as heart rates, survival and hatching rates, were recorded at different time intervals.

2.6. In vivo tracing of GQDs and USGO

N-GQDs exposed zebrafish embryos at 48 hpf and 72 hpf were respectively observed under UV light excitation (330–380 nm) using an invert fluorescent microscope (NiKon SMZ18, Japan). To avoid the adverse effects of UV light on organisms, zebrafish embryos for different treatment were scanned by UV light for less than 300 ms. To track USGO biodistribution in zebrafish, the as-prepared FITC-BSA-conjugated GO (0.3 mg/mL) was pipetted into 6-well plates containing zebrafish embryos, and then incubated for 0.5 h in the dark. The real-time monitoring of USGO movement was carried out using a confocal laser scanning microscopy (CLSM, FV1200, Olympus, Japan).

2.7. In vitro and in vivo assessment of reactive oxygen species (ROS)

In vitro cell-free detection of ROS signal was performed according to the previously reported method [36]. ROS levels in zebrafish embryos were quantified according to the methods described in previous studies [37–39]. In brief, 35 embryos per treatment at 3dpf, 4 dpf, and 5 dpf, were prepared for different exposure concentration of NPs. Each treatment including control was performed for three biological replicates, and the total fluorescence for various groups was calculated as Mean ± SEM.

2.8. Biochemical analysis

After exposure for 6 d, 50 zebrafish per treatment were sampled for the determination of enzymatic activities of catalase (CAT), superoxide dismutase (SOD), and glutathione peroxidase (Gpx). Firstly, the collected fish were anesthetized with 0.05% (w/v) MS-222 solution, and then homogenized with 0.9% physiological saline (w/v) on ice. The homogenate (1: 10 w/v) was centrifuged at 3000 × *g* for 10 min at 4 °C, and then the supernatant was collected for enzymatic activity assays. Each treatment was performed for three biological replicates. Based on the chemical reaction between hydrogen peroxide and ammonium molybdate, CAT activities were measured by spectrophotometric to detect the pale-yellow end-product at 405 nm in pH 7.0 sodium phosphate medium. Hydroxylamine method was employed to detect the total SOD activities, and GSH-Px (GPx) activities were determined by the yellow end-product at 412 nm, which was produced by the interaction between GSH and 5,5′-Dithiobis-(2-nitrobenzoic acid) (DNTB). Activities of these three enzymes were determined and calculated with assay kits (Institute of Biological Engineering of Nanjing Jianchen, Nanjing, China) as A007-1-1, A001-1-1, and A005, respectively. In addition, we made an *in vitro* cell-free enzyme activity assay for CAT to check whether CAT activities on hydrogen peroxide are changed by NPs. The chemical assays were carried out according to the previously described method [40]. In brief, 50 mM hydrogen peroxide was prepared as the catalytic substrate for catalase and N-GQDs. The final concentration of catalase solution was prepared as 20 U/mL by dissolving 0.05 mg catalase powder into 10 mL E3 solution. Four concentrations of NPs solutions were prepared as 25, 50, 100, and 200 μg/mL, respectively, and E3 solution was set as the control group. After the reaction, the final catalase activities were determined by a catalase assay kit (A007-1, Nanjing Jiancheng Bioengineering Institute, China).

Several NADPH dehydrogenases of the respiratory chains were involved in the redox reaction and conducted the oxidative process of NADH (P) to NAD (P). In this study, enzymatic activities of three typical mitochondrial respiratory chain complexes (complex I, complex III, and complex IV) were investigated. Activities of these enzymes were determined in similar sampling ways to the bioassays for CAT/SOD/Gpx. The activities of complex I, III, and IV were detected using specific kits BC0510, BC 3240, and BC0940 (Solarbio, Beijing, China), respectively. All data were indicated as Mean ± SD, $^{*}p < 0.05$.

2.9. o-dianisidine staining

o-dianisidine staining was used to detect the mature hemoglobin levels in zebrafish embryos that were exposed to NPs, and the procedure of the *o*-dianisidine staining was performed as described [41]. Briefly, the NPs exposed zebrafish embryos at 36 hpf were placed into 6-well plates, washed with clean water, and then incubated with an *o*-dianisidine solution for at least 15 min. After dyeing, zebrafish embryos were washed with clean water and observed using an inverted microscope (Nikon SMZ18, Japan). Hemoglobin levels were marked by rust-colored precipitates, which were specifically labeled for hemoglobin in erythroid cells.

2.10. Immunohistochemical analysis

To further determine N-GQDs bio-distribution and associated injured regions, tunnel assays were performed in zebrafish embryos exposed to NPs at 72 hpf. Firstly, whole-mount paraffin-embedded zebrafish were processed by following the steps of cutting, paraformaldehyde (4%) fixation, and paraffin embedding. Serial slices with an average thickness of 4 μm were performed. After that, white paraffin-embedded slices were directly observed under UV light excitation (330–380 nm) using the stereo-fluorescence microscope. Tunnel assay was performed using DeadEnd™ Colorimetric TUNEL System (Promega, USA) according to the manufacturer's protocol.

2.11. AO/EB double staining

To detect the apoptosis in NPs exposed zebrafish, AO/EB double staining was performed as described [42–44]. Acridine orange (AO) and ethidium bromide (EB) were prepared to uniformly mix with the final concentration of 100 μg/mL, and zebrafish embryos were immersed in AO/EB solution for 30 min at 28 °C and covered with silver papers. After washing three times with 1 × PBS, zebrafish were carefully pipetted into glass slides and observed with 10 × CLSM. The number of apoptotic areas (infectious loci) was counted and analyzed by Image-Pro Plus 6.0 software.

2.12. Whole-mount in situ hybridization (WISH)

Zebrafish exposed to 100 μg/mL NPs at different developmental stages were collected for WISH analysis. Four probes (*hbbe1*, *tfa*, *cyp1a*, and *mpx*) were used in the study, and WISH was performed according to the online protocols (http://zfin.org/ZFIN/Methods/ThisseProtocol.html). Primer pair sequences were designed according to the previous reports [41,45–48].

2.13. Immunoblotting analysis

The primary antibodies of zebrafish Casp8 (GTX54181) and Casp3 (GTX54182) were purchased from Genetex (Irvine, CA, USA) for detecting NPs induced Caspase-related apoptosis in zebrafish at 6 dpf. Immunoblotting assays were performed according to the standard protocols. Protein samples from control and zebrafish exposed to different concentrations of GQDs (50 μg/mL, and 100 μg/mL) and USGO (100 μg/mL) were extracted for WB analysis. Bradford assay protocol was used to measure the total protein content in the embryonic cell lysate [49]. Mouse monoclonal antibody against β-Tubulin (Earthox, LLC, E021160-03) was used as a loading control.

2.14. qPCR analysis

Quantitative real-time PCR (qPCR) was carried out using ABI ViiA 7™ real-time PCR system (Applied Biosystems, Carlsbad, CA, USA) with SYBR® Premix Ex Taq™ II (Perfect Real Time, Takara). RNAs isolated from zebrafish samples at different treatment were used for cDNA synthesis. The first-strand cDNAs were transcribed with PrimeScript™ RT reagent kit with gDNA eraser (Takara, Dalian, China) according to the manufacturer's instructions, and 1 μg of the total mRNAs were prepared for the cDNA synthesis. Running a program of qPCR was initiated from 95 °C, incubating for 5 min, followed by 40 cycles of 95 °C for 15 s, 60 °C for 30 s, 72 °C for 30 s. Primers were designed by Beacon Design 8 (Table 1), and *β-actin* were selected as the internal control to normalize the relative mRNA levels [50]. Three independent biological replicates were performed for each treatment, and $2^{-\Delta\Delta Ct}$ method was used to quantify gene expression levels.

Table 1
Primers used for quantitative real-time PCR in this study.

Gene name	Accession No.	Forward primer (5′–3′)	Reverse primer (5′–3′)	Amplified length (bp)
β-actin	NM_131031	ACGAGAGATCTTCACTCCCCT	TGCCAACCATCACTCCCTGA	189
cat	NM_212846	GCAGAGGGCTTTGATTGTGT	AATCACGATGGTCAGGCAGT	259
hbbe2	NM_212846	GACATCAAGAACACCTACG	AGAGCAGAGACAACAACA	185
cyp1a	NM_131879	AAGTTGGAAGGCGAGAAGG	GCCAGGAACAGGAAGACTTC	95
ahrr1	NM_001035265	TTACTGGACAGCACCTCT	GGCTCCTCATCTTCAGATC	172
ahrr2	NM_001033920	GCTTCCACAAACACAACT	TCTCATCATCCACTTCATACT	81
mpx	NM_212779	TCGTGTCAATGAGAATCCT	CCTACAATTAGTGGCAAGTATT	192
tfa	NM_001015057	CGATATGATTGAGAGGACCTA	TATGACTGTTTGATGTGTTTGA	127

2.15. Statistical analysis

Statistical analysis was carried out with SPSS 19.0 software (IBM, USA), and significant differences between control and treatment were determined by independent sample *t*-test or one-way analysis of variance (ANOVA), following by a post hoc test (Tukey's method) with significant levels as following: $^{*}p < 0.05$, $^{**}p < 0.01$, and $^{***}p < 0.001$.

3. Results

3.1. NPs characterization

As shown in Fig. 1A, the image of the transmission electron microscope (TEM) showed that the sizes of N-GQDs nanoparticles distributed between 1 and 9 nm, and 80% of the fabricated N-GQDs distributed with sized 3–7 nm. The TEM image of ultrasmall GO (USGO) showed that > 80% USGO nanoparticles were flakes with the lateral size distribution in the nanosize of < 50 nm (Fig. 1C). Furthermore, AFM images indicated that the morphologies of N-GQDs and USGO were nanoscale, and the AFM results showed the lateral size distribution (Fig. 1B and D). The height size distributions of N-GQDs and USGO were about ~1 nm and ~1.5 nm, respectively. As shown in Fig. 1E, the zeta potential of USGO and N-GQDs was both negatively charged in three mediums, including ultrapure water (ddH_2O_2), 1 × PBS (pH 7.4), and DMEM. In contrast to USGO nanoparticles, the zeta potential of N-GQDs decreased greatly from water to the other two mediums, showing the enhancing flocculation of N-GQDs in PBS and DMEM mediums. Meanwhile, XPS analysis was performed to confirm the functional groups on the surface of N-GQDs and USGO (Fig. 1F–G). The detail about the GQDs chemical characterization was discussed in our previous paper [10]. The prepared USGO contains 73.85% C1s (282.38–297.98 eV), 21.39% O1s (530.62–544.98 eV), and 2.14% N1s (398.69–409.98 eV). The result of FTIR showed similar characteristic peaks between GO and USGO (Fig. S1).

3.2. High concentration of N-GQDs arrested zebrafish development

Like our previous study [10], the hatching rate of zebrafish declined after exposure to 100 μg/mL concentration of N-GQDs at 96 hpf, but not to a significant level when compared to control groups (Fig. 2A). The mortality rate at 96 hpf showed no significant changes among different treatments (Fig. 2B). Heartbeat rates at 96 hpf declined slightly with a concentration-dependent manner of N-GQDs (Fig. 2C). USGO exposed groups revealed no significant changes for various developmental indices, even at the highest exposure concentration (100 μg/mL). Interestingly, the highest concentration of N-GQDs (100 μg/mL) significantly increased the malformation rates in zebrafish at 120 hpf, compared to that in USGO exposed groups (Fig. 2D). Bent spine (BS) and reduced pigmentation were clearly observed in both GQDs and USGO exposed zebrafish larvae, compared to the control group (Fig. 2E–G).

3.3. N-GQDs exhibited strong permeable effects in zebrafish embryos

In our previous study, the biodistribution of N-GQDs in zebrafish was well characterized in terms of the wide-range of fluorescence signals emitted by N-GQDs under different excitation wavelengths, *i.e.* blue, green, and red [10]. In this study, we found that N-GQDs exposed zebrafish exhibited fluorescence enhancement effects in a short UV excitation time (< 300 ms), compared to that of the other two photoluminescence (> 1 s). Based on that, we found that N-GQDs possess strong permeable effects in zebrafish embryos that were easily distinguished under the inverted fluorescence microscope. Further, a difference was observed in biodistribution characteristics of N-GQDs across the development of zebrafish embryos (Fig. 3). In zebrafish embryos at 48 hpf, the bio-accumulative effects of N-GQDs mainly occurred in the region near to the common cardinal veins and tail veins (Fig. 3A-a2), implying an uneven distribution pattern inside the embryo. However, in zebrafish embryos at 72 hpf, N-GQDs showed fluorescence enhancement effects in the caudal region and in the area adjacent to the circulatory system (Fig. 3A-a4 and Fig. S2). Moreover, the use of *fli1a*: EGFP transgenic zebrafish in N-GQDs exposure gave a more direct sight of flow effects of N-GQDs around the dorsal aorta (DA) and caudal venous plexus (CVP) (Fig. 3B-b5 and b6). However, compared to the weak fluorescence background in control group (Fig. 3C and E), FITC-labeled USGO exposed zebrafish embryos were decorated with intense green fluorescence, in which USGO mainly distributed in the surface areas of head, notochord, and tail of zebrafish embryos at 48 hpf (Fig. 3D), and spread along the intestinal tract at 72 hpf (Fig. 3F).

3.4. N-GQDs inhibited ROS generation in zebrafish embryos

In vitro cell-free assays showed that DCF fluorescent intensity decreased slowly when the exposure concentration of N-GQDs increased, but USGO induced very high fluorescence, even at the lowest concentrations (0.5 μg/mL) (Table 2), implying that N-GQDs possessed the weak potential for ROS generation. *In vivo* bioassays revealed the similar changes of ROS levels in N-GQDs exposed zebrafish. Further, when the exposure time was prolonged, ROS levels decreased significantly in N-GQDs exposed zebrafish (Fig. 4). In contrast, at the same exposure concentrations, USGO induced stronger fluorescent intensity than N-GQDs and control zebrafish at 4 dpf, but quickly decreased at 5 dpf, when compared to control groups.

3.5. N-GQDs selectively inhibited antioxidant enzyme activities

In vitro cell-free assays demonstrated that N-GQDs can compete with CAT for decomposing H_2O_2, while USGO has no significant inhibitory effects on CAT activities (Fig. 5A). Compared to control and USGO exposed zebrafish, CAT activities in N-GQDs decreased slowly in a concentration-dependent manner, and reduced to a significant level in 100 μg/mL N-GQDs treated groups, indicating that N-GQDs can competitively inhibit CAT to decompose H_2O_2. Instead, CAT activities increased significantly in 100 μg/mL USGO exposed zebrafish (Fig. 5B). *In*

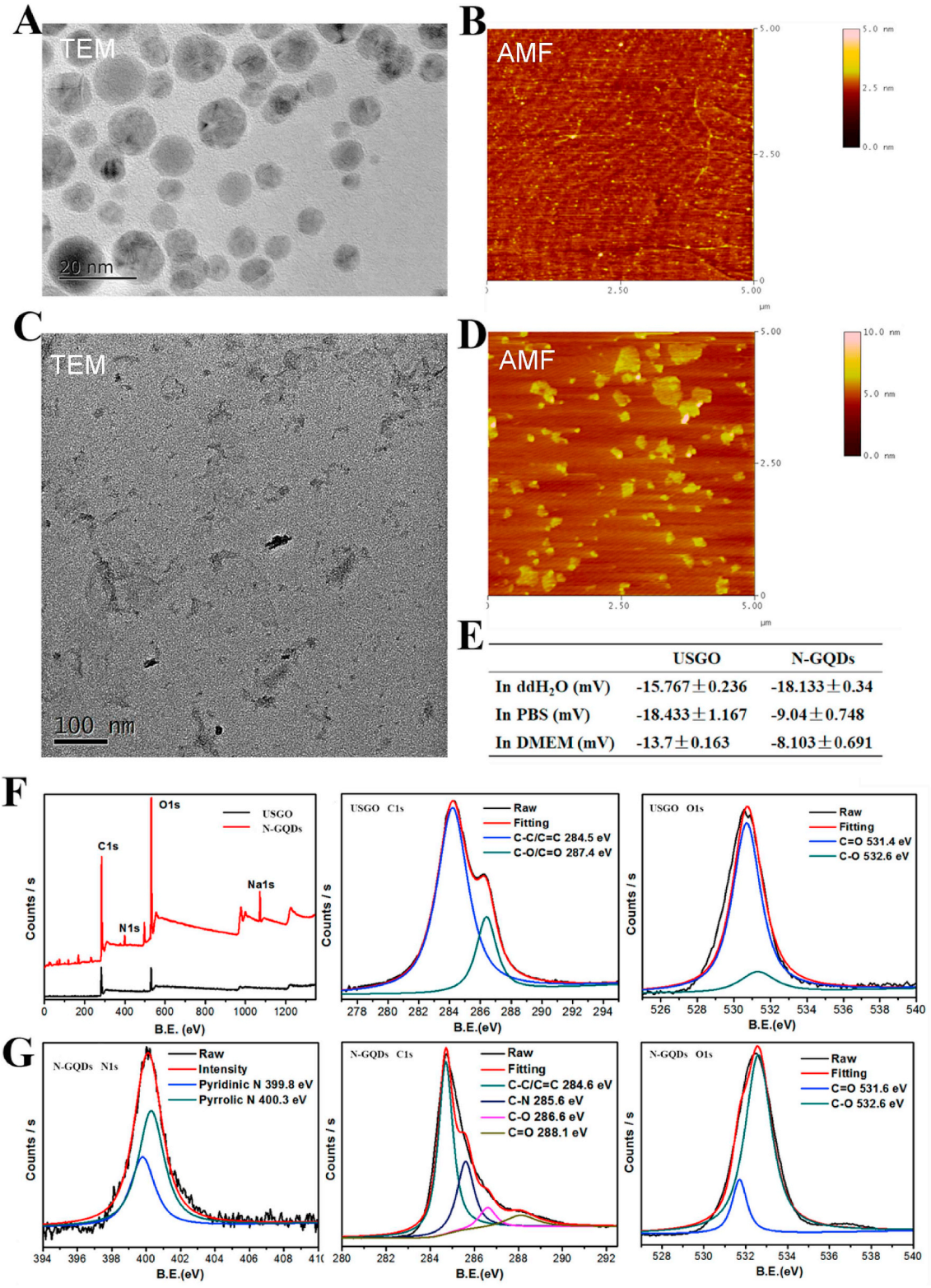

	USGO	N-GQDs
In ddH_2O (mV)	-15.767±0.236	-18.133±0.34
In PBS (mV)	-18.433±1.167	-9.04±0.748
In DMEM (mV)	-13.7±0.163	-8.103±0.691

Fig. 1. Surface characterization of N-GQDs and USGO. (A–B) TEM and AFM images of N-GQDs (scale bar = 20 nm). The inset in Fig. 1A shows the lateral size distribution (counted number: 100) and the inset in Fig. 1B demonstrates the height size distribution. (C–D) TEM and AFM images of USGO (scale bar = 100 nm). (E) Zeta potential of USGO and N-GQDs in three mediums, including ddH_2O_2, 1 × PBS (pH 7.4), and DMEM, each treatment was performed for three replicates (Mean ± SEM). (F) and (G): XPS characterization of USGO and N-GQDs.

vivo assays showed that SOD activities were also repressed in N-GQDs exposed zebrafish, and decreased to a significant level, when the exposure concentration of N-GQDs was 100 μg/mL (Fig. 5C), but SOD activities were remarkably elevated in 100 μg/mL USGO exposed zebrafish. Interestingly, we found that GPx activities in N-GQDs exposed zebrafish increased significantly when compared to the other two treatments, and no significant differences were observed between control and USGO exposed groups (Fig. 5D). Unlike SOD and GPx that

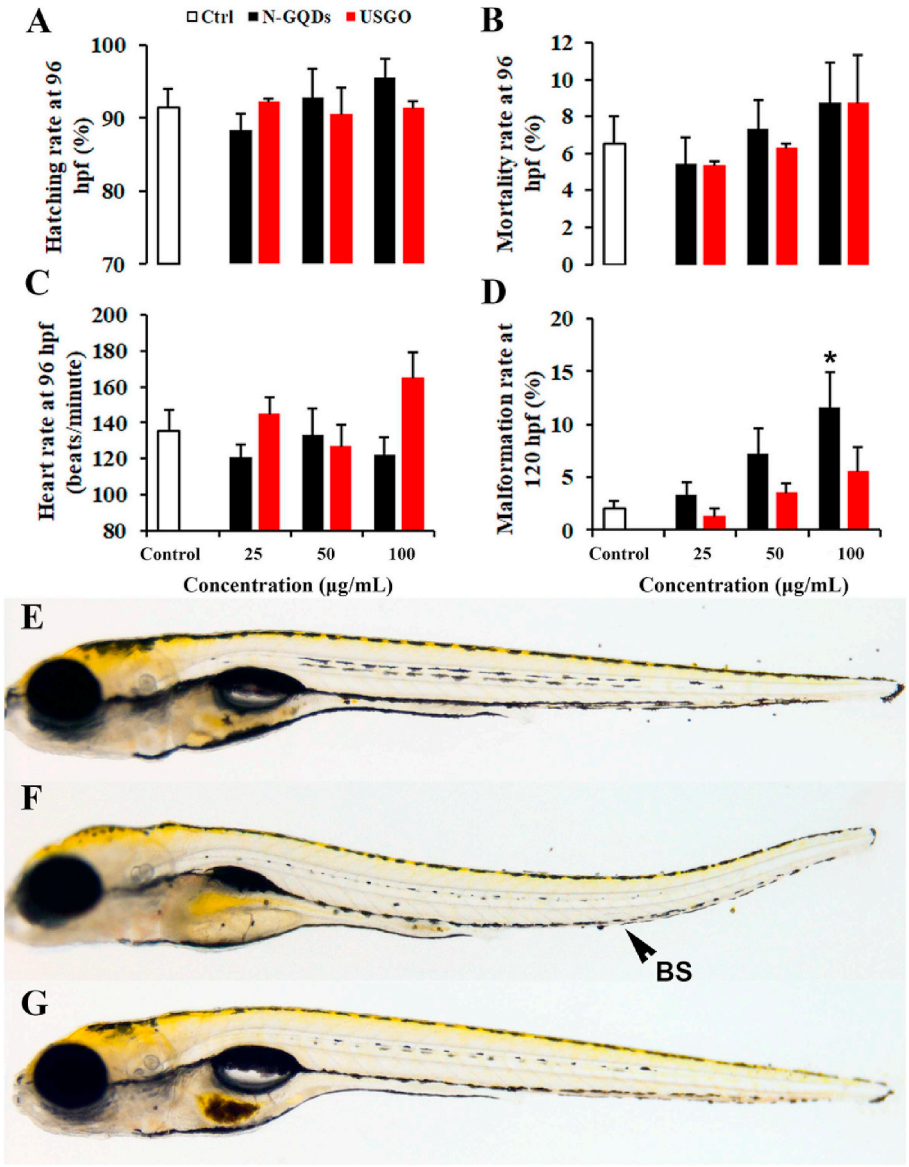

Fig. 2. Developmental indices of zebrafish exposed to N-GQDs and USGO. (A–D) Statistical results of hatching rates (96 hpf), mortality rate (96 hpf), heart rate (96 hpf), and malformation rate (120 hpf) of zebrafish after exposure to N-GQDs and USGO at different exposure concentrations. Images showed zebrafish larvae in the control group (E), 100 μg/mL N-GQDs group (F), and 100 μg/mL USGO group (G). The black arrow indicated the developmental malformation (bent spine, BS) in N-GQDs exposed zebrafish at 120 hpf.

are polymorphic in genetic structures and possess more than two isoforms in zebrafish, CAT is translated from only one transcript, indicating that the transcription levels of catalase (*cat*) are stably expressed than the other two antioxidant enzymes. Accordingly, qPCR was performed to check the *cat* expression levels in parallel with the enzyme activities assays. The result showed that *cat* mRNA levels were not significantly changed in N-GQDs exposed zebrafish at 3 dpf, but greatly decreased after exposure to N-GQDs for 6 d, which showed a concentration-dependent effect; however, USGO revealed no regulatory effects on the *cat* expression levels (Fig. S3).

3.6. N-GQDs exerted inhibitory effects on mitochondrial respiratory chains

Mitochondrial respiratory chains (MRCs) are an orchestra of protein complexes that are responsible for transferring electrons from donor molecules to acceptor molecules *via* the redox reaction. There are three important proton pumps simultaneously operating in MRCs: complex I, complex III, and complex IV, which function as ion carriers to reduce molecular oxygen to water. Here we found that all enzyme activities in the two MRCs of complex I complex II, and complex III were relatively reduced in N-GQDs exposed groups, but the enzyme activities of complex IV were not markedly changed after N-GQDs treatment. On the contrary, the relative enzyme activities of the three enzymes were greatly elevated in USGO exposed groups (Fig. 6).

3.7. N-GQDs selective repressed hemoprotein activities

Hemoglobin (Hb) is a member of a superfamily of hemoproteins that are involved in the transportation of oxygen (O_2) in vertebrate organisms [51]. Elevated levels of hemoglobin are usually associated with an increase of red blood cells [52]. Besides functioning as an oxygen carrier, Hb is proved to have the capacity of redox chemistry, especially under some unfavorable stresses [53]. At 36 hpf, the rust-colored precipitates marking for Hb levels were found much less in N-GQDs exposed zebrafish than that in control and USGO exposed zebrafish. Accordingly, the mRNA levels of hemoglobin-2 (*hbbe2*) were also detected

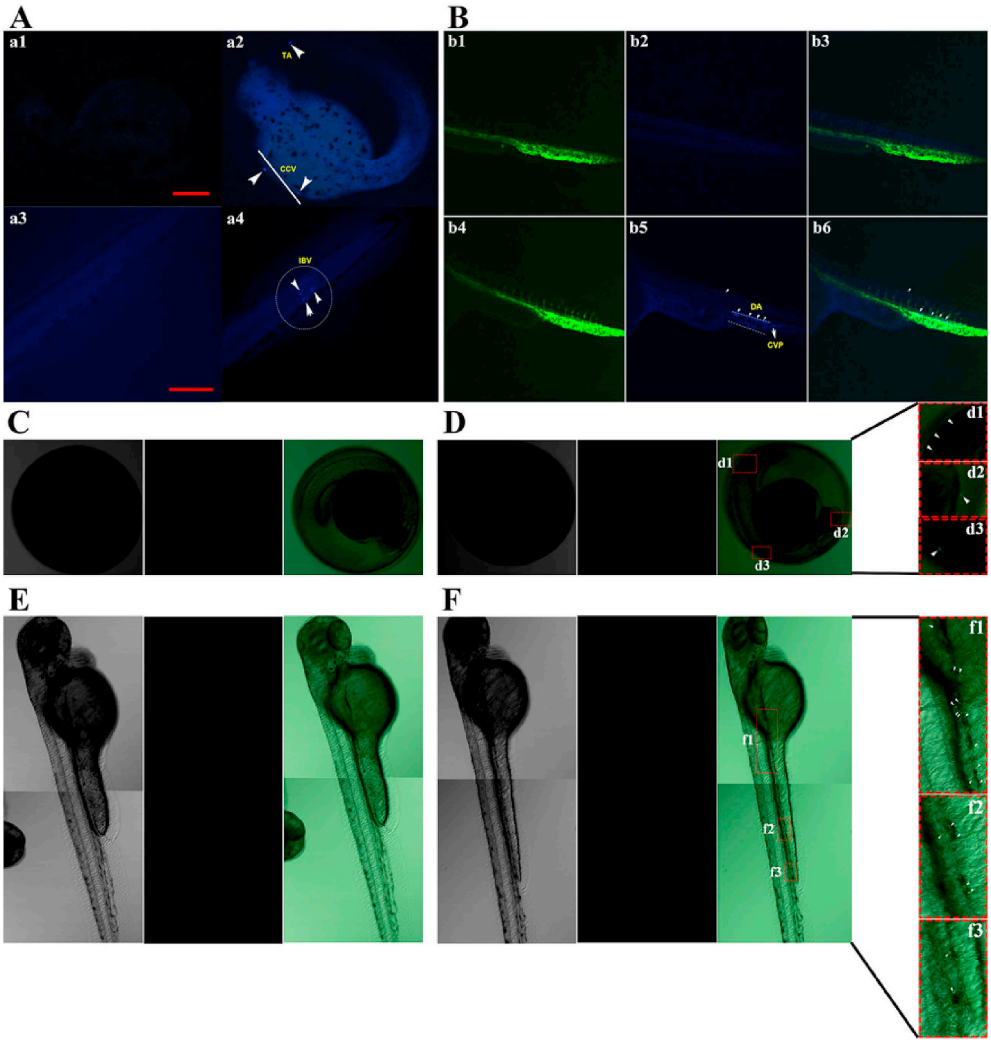

Fig. 3. Distribution of N-GQDs and FITC-BSA labeled USGO (FITC-USGO, 1 mg/mL) in zebrafish embryos at 48 hpf and 72 hpf. (A) Zebrafish embryos at 48 hpf after exposure to 100 μg/mL N-GQDs solution. White arrows indicated the permeable effects of N-GQDs around the circulatory system (TA: tail artery, CCV: common cardinal vein, IBV: intersegmental blood vessel). Images were captured under the inverted fluorescence microscope, scale bar = 250 μm a1-a4 showed the whole and regional profiles of the wild-type zebrafish embryos under the excitation of 380 nm wavelength with or without NPs treatment. a1 and a3: control zebrafish; a2 and a4: NPs exposed zebrafish. (B) The dynamic changes and permeable effects of N-GQDs in transgenic zebrafish embryos (*fli: eGFP*) at 72 hpf after exposure to 100 μg/mL N-GQDs. White arrows indicated the dynamic flow of N-GQDs along the dorsal aorta (DA). Images were real-time captured under 10XCLSM. b1-b3: control zebrafish, b1 and b2 were the images captured under the excitation of 480 nm and 405 nm wavelength, respectively, and b3 was the merged image of b1 and b2. b4-b6: NPs exposed zebrafish embryos. and b4-b6 were acquired under the same conditions to b1-b3. (C–F) Visualization of FITC-labeled USGO in zebrafish embryos at 48 h and 72 h under 10XCLSM. The green fluorescent spots indicated by white arrows showed the biodistribution of USGO in zebrafish. C and E were both control zebrafish embryos at 48 h and 72 h, respectively. D and F were NP exposed zebrafish embryos at 48 h and 72 h, respectively. d1-d3 and f1-f3 indicated the biodistribution of the FITC-labeled USGO in zebrafish embryos at 48 h and at 72 h, respectively. (For interpretation of the references to color in this figure legend, the reader is referred to the Web version of this article.)

to be significantly up-regulated in N-GQDs exposed zebrafish based on WISH results (Fig. 7A). Further, when the exposure time extended to 6 dpf, *hebb 2* mRNA levels maintained a relatively low expression level when compared to the other two treatments (Fig. 7B). In addition, we checked two typical hemoproteins: myeloperoxidase (*mpx*) and one cytochrome P450 monooxygenase (*cyp1a*), which are responsible for producing hypohalous acids against microbes and metabolizing various physiologic and xenobiotic organic compounds, respectively. Here we confirmed by WISH that the mRNA levels of *mpx* mainly expressed in the hindbrain, spinal cord, as well as the cardinal veins. However, the staining in the posterior cardinal vein was greatly reduced in N-GQDs exposed zebrafish at 3dpf and 4 dpf, respectively (Fig. 7C), and did not recover the normal expression levels at 6 dpf (Fig. 7F). However, the expression level of *cyp1a* was identified to be slightly induced in livers in both NPs exposed zebrafish at 3 dpf (Fig. 7D), and remained to be highly activated at 6 dpf (Fig. 7F). The higher activation levels of Cyp1a were also examined in the transgenic zebrafish *Tg (cyp1a: eGFP)* after exposure to N-GQDs (Fig. S4). In addition, the transcriptional levels of *ahrr1* and *ahrr2* were found to be significantly changed after exposure to NPs, implying the formation of AhR/AhRR feedback loop model occurred in NPs exposed zebrafish (Fig. 7F).

Based on the above analysis, we investigated the total iron binding capacity using a molecular marker, transferrin a (TFA). At 3dpf, the result of WISH showed that there were no significant changes of *tfa* mRNA levels between control and NPs exposed zebrafish (Fig. 7E), but qPCR results demonstrated that *tfa* mRNA levels increased sharply after exposure to N-GQDs for 6 d (Fig. 7F).

Table 2
NPs induced ROS signals *via* cell-free assay.

Treatment	Control	E3	N-GQDs USGO			
			0.5 μg/mL	1 μg/mL	2 μg/mL	4 μg/mL
DCF fluorescence (units) Data ± SEM	23, 366 ± 4, 567	24, 446 ± 3, 256	20, 399 ± 945 68, 823 ± 7, 657	24, 167 ± 2532 95, 235 ± 13, 782	23, 696 ± 1, 935 122, 329 ± 9, 017	20, 457 ± 645 186, 125 ± 22, 338

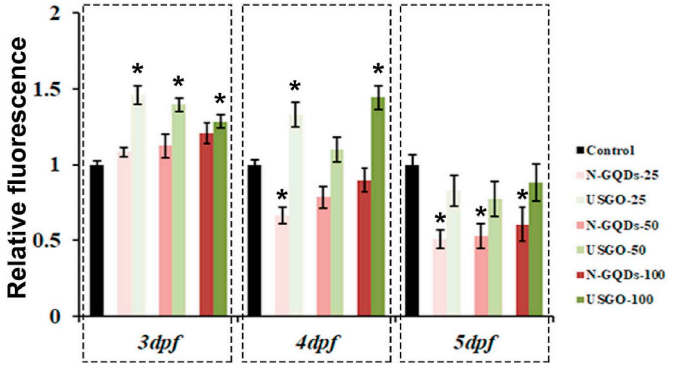

Fig. 4. *In vivo* ROS levels in zebrafish embryos exposed to N-GQDs and USGO. Statistical comparison of the absolute fluorescence (units) in embryonic cells exposed to both NPs. Zebrafish embryos at 3, 4, and 5 dpf that exposed to the concentration gradient of NPs solution (0-25-50-100 μg/mL) were collected for ROS detection. Each exposure concentration was performed for three replicates (n = 35 individuals per replicate). Significant analysis among various treatment was performed by means of one way ANOVA, $^{*}p < 0.05$, $^{**}p < 0.01$, $^{***}p < 0.001$.

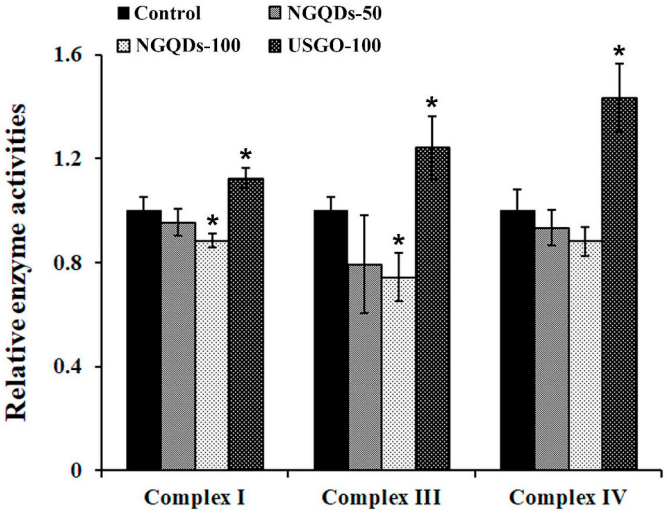

Fig. 6. Enzymatic activities assays for mitochondrial respiratory chain complex. Each concentration was performed for three independent replicates (n = 50 embryos per replicate). Values were calculated by the ratios between treated and control groups, which are indicated by Mean ± SEM.

3.8. N-GQDs induced higher levels of apoptosis than USGO

The observation of white paraffin-embedded section under the UV light excitation revealed the accumulative effects of N-GQDs in zebrafish embryos at 96 hpf, mainly distributing in the yolk sac, the region near to eyes and along the intestinal tract (red arrows in Fig. 8A: a4), most of which were basically in accordance with the earlier findings obtained in this study (Fig. 3A–B). The accompanied tunnel assays showed that both NPs exposed zebrafish underwent apoptosis, but N-GQDs induced more apoptosis (indicated by brown granules) in the areas of the hindbrain, hindgut, and around the notochord than that in USGO exposed zebrafish at the same exposure concentration (100 μg/mL) (Fig. 8A: a3). USGO induced apoptosis mainly aggregating in the regions around eyes and also along the foregut (Fig. 8A: a5), which is basically in agreement with USGO biodistribution in zebrafish embryos (Fig. 3D and F). The result of AO/EB staining further confirmed that N-GQDs caused considerable apoptosis at 100 μg/mL than the other two treatments in zebrafish, and apoptosis was observed between dorsal stripe and ventral strip at 96 hpf, mainly covering the intersected regions of the tail artery and caudal veins (Fig. 8B). Accordingly, tunnel assays and A/B double staining further strengthen the findings of NPs mediated apoptosis in different regions of zebrafish body: region-1 (R1), region-2 (R2), and region-3 (R3) (Fig. 8C). Statistical data showed that both NPs had adverse effects on R1 and R3, and only N-GQDs exert significantly toxic effects on R2. Comparatively, N-GQDs induced more apoptosis than USGO in R3 (Fig. 8C and Fig. S5-S6). WB analysis showed concentration-dependent effects of N-GQDs on the expression of Casp8 and Casp3, and N-GQDs induced relatively higher expression levels of Casp8 and Casp3 than USGO at the same exposure concentration (Fig. 8D–E).

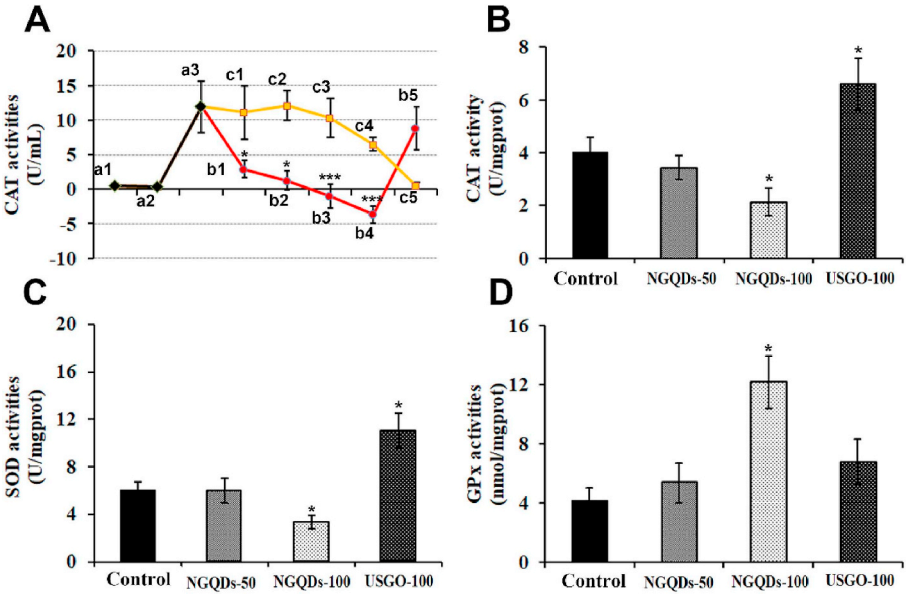

Fig. 5. Enzymatic activities assays for CAT, SOD, and Gpx. (A) *In vitro* cell-free assays for the detection of CAT activities when catalase mixed with hydrogen peroxide (H_2O_2), and supplemented with various concentrations of NPs. a1: control (E3 solution), a2: control + 50 mM H_2O_2, a3: catalase solution (20 U/mL) + 50 mM H_2O_2; b1: catalase solution (20 U/mL) + 50 mM H_2O_2 + 25 μg/mL N-GQDs, b2: catalase solution (20 U/mL) + 50 mM H_2O_2 + 50 μg/mL N-GQDs, b3: catalase solution (20 U/mL) + 50 mM H_2O_2 + 100 μg/mL N-GQDs, b4: catalase solution (20 U/mL) + 50 mM H_2O_2 + 200 μg/mL N-GQDs, b5: 50 mM H_2O_2 + 200 μg/mL N-GQDs; c1: catalase solution (20 U/mL) + 50 mM H_2O_2 + 25 μg/mL USGO, c2: catalase solution (20 U/mL) + 50 mM H_2O_2 + 50 μg/mL USGO, c3: catalase solution (20 U/mL) + 50 mM H_2O_2 + 100 μg/mL USGO, c4: catalase solution (20 U/mL) + 50 mM H_2O_2 + 200 μg/mL USGO, c5: 50 mM H_2O_2 + 200 μg/mL USGO. (B–D) showed the activities of CAT, SOD, and GPx in control and NPs exposed zebrafish at 6 dpf, respectively. Data were represented as Mean ± SEM, and independent-samples *t*-test was used to compare control and NPs treated groups. Each concentration was performed for three replicates (n = 50 embryos per replicate), $^{*}p < 0.05$, $^{**}p < 0.01$, $^{***}p < 0.001$.

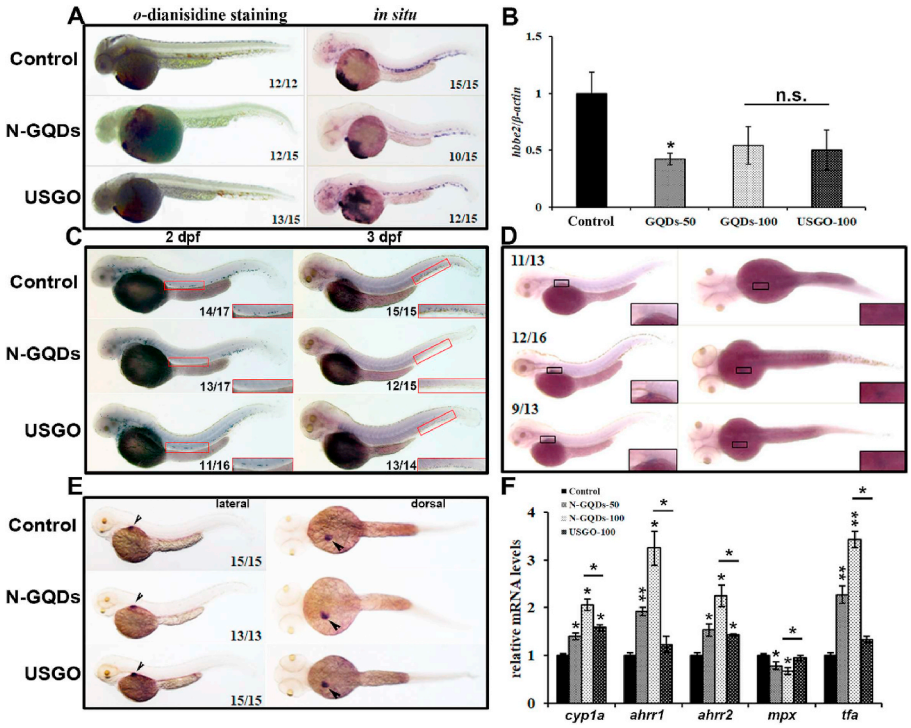

Fig. 7. Molecular detection of Hb, *hbbe2*, *mpx*, *cyp1a*, *tfa*, and *ahrr* in NPs exposed zebrafish at different time points. (A) The changes of Hb (*o*-dianisidine) and its mRNA expression levels in zebrafish embryos exposed to NPs at 36 hpf. (B) The mRNA expression levels of *hbbe2* in zebrafish exposed to NPs at 6 dpf. (C) The mRNA expression levels of *mpx* in zebrafish exposed to NPs at 2 dpf and 3 dpf, respectively. (D) The mRNA expression levels of *cyp1a* in zebrafish exposed to NPs at 3 dpf. (E) The mRNA expression levels of *tfa* in zebrafish exposed to NPs at 3 dpf, and black arrows indicated the expressed regions of *tfa*. (F) The mRNA expression levels of *cypa 1*, *ahrr1*, *ahrr2*, *mpx*, and *tfa* in zebrafish exposed to NPs at 6 dpf. Comparative analysis of gene expressions between NPs and controls was statistically performed by independent-samples *t*-test, and values were represented by means ± SEM, $^{*}p < 0.05$, $^{**}p < 0.01$.

4. Discussion

GQDs hold great promises for its huge extensive applications in bioengineering, such as bioimaging, biosensors, drug delivery, and anticancer adjuvants. The accurate biosafety evaluation of GQDs using *in vivo* system can assist us to unveil the potential molecular perturbation induced by these NPs. Therefore, the current study showed that N-GQDs have strong peroxidase-like activities in eliminating free radicals and selectively inhibiting the endogenous antioxidant enzyme activities.

The surface characterization showed that N-GQDs inherit some

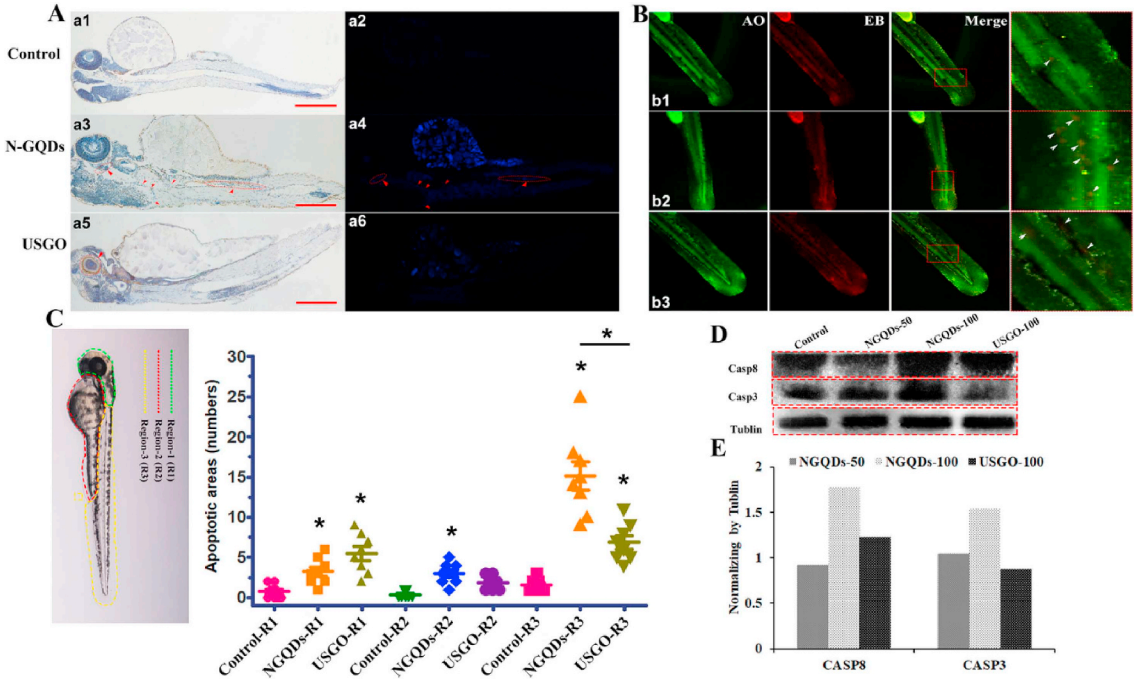

Fig. 8. Molecular detection of Hb, *hbbe2*, *mpx*, *cyp1a*, *tfa*, and *ahrr* in NPs exposed zebrafish at different time points. (A) a1 (control), a3 (N-GQDs), and a5 (USGO) were the photographs of tunnel assays for NPs exposed zebrafish at 72 hpf,. a2, a4, and a6 were the images of white paraffin-embedded slices under UV excitation wavelength (330–380 nm). (B) AO/EB double staining indicated the apoptosis induced in zebrafish embryos that exposed to NPs (100 μg/mL) for 72 h under 10 × CLSM. Comparison between control and treatment was carried out by independent-samples *t*-test, and values were represented by means ± SEM, $^{*}p < 0.05$, $^{**}p < 0.01$, $^{***}p < 0.001$. (C) Statistical results of NPs induced apoptosis in different regions in zebrafish: R1 (green dot line), R2 (red dot line), and R3 (yellow dot line). (D) Western blotting for Casp8 and Casp3a in zebrafish after exposure to NPs for 6 d. (E) Casp8 and Casp3 were normalized against β-Tubulin according to the intensity of the WB bands. (For interpretation of the references to color in this figure legend, the reader is referred to the Web version of this article.)

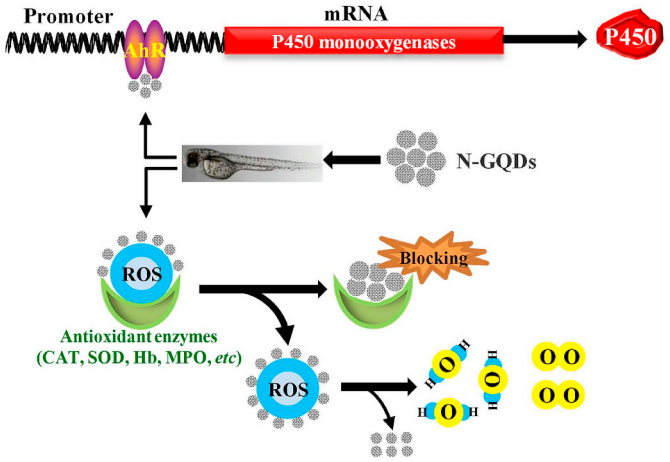

Fig. 9. A schematic depiction of the bilateral effects of N-GQDs on antioxidant enzyme.

physicochemical properties from parent G [10], and also share fluorescent characters with other sources of GQDs [5] (*e.g.* nitrogen-free GQDs). However, N-GQDs emit intense blue PL that is totally different from the green PL of their nitrogen-free counterparts [54]. Except for the size and surface effects of N-GQDs, the oxygen-rich functional groups are an important contributor for its excellent blue luminescence [54,55]. Therefore, the fluorescence enhancement effects rendered us feasibility to determine the permeable effects of N-GQDs in zebrafish embryos.

The low toxicity of GQDs was mainly confirmed using *in vitro* systems [15–22], but it is less reported for *in vivo* systems [22,33,56]. Also, the systemic evaluations of GQDs remain largely unexplored due to the limited detection of biochemical indicators in cells and mice. Moreover, the toxicity data from various cohorts that exposed to GQDs are very scarce. In contrast to murine models, zebrafish show more advantages in phenotype observation, genetic manipulation, and sampling. In this study, the developmental coordination between the N-GQDs exposed and control groups showed a relatively high proportion of malformation-'bent spine' in N-GQDs treated zebrafish. The large-scale sampling from different treatments provided the direct insight to the changes in the levels of ROS and associated antioxidant enzymes (*e.g,* CAT, SOD, and GPx), which are conventionally examined *in vitro* in previous studies.

CAT, SOD, and GPx in organisms, mainly act as antioxidant enzymes to detoxify ROS signals including superoxide anion, hydrogen peroxide, singlet oxygen, and hydroxyl radicals, which are usually generated as the byproducts from cell metabolism [57–59]. It has been reported in previous studies that G and its derivatives (CNTs and GO) can activate the enzyme activities of CAT, SOD, and GPx *in vitro* or *in vivo*, all of which were usually generated along with the large amount of ROS induced by these NPs [60–70]. Here, we found that USGO basically inherited the biochemical properties from GO, which can stimulate ROS generation and enhance *in vivo* antioxidant enzyme activities.

Due to the intrinsic antioxidant enzyme-like catalytic activities, N-GQDs have been proven effective in scavenging free radicals and thereby protecting cells against oxidative damages [55,71]. Our findings revealed that N-GQDs cannot trigger ROS signals, instead of retarding its generation *in vivo* system, in contrast to the characters of GO. The side effects of N-GQDs on antioxidant enzyme cannot be ignored, and the previous reports indicated that the appropriate concentrations of H_2O_2 can induce the gene expression related to development, reproduction and regeneration in zebrafish [72,73]. Furthermore, we found that N-GQDs selectively exerted inhibitory effects on the antioxidant enzyme, and then likely affect the natural immune system. Some previous studies have shown that few anti-inflammatory drugs (*e.g,* indomethacin) used for scavenging free radicals could imperil the endogenous peroxidase, leading to the irreversible injuries *in vivo* systems [74,75]. *In vitro* assays indicated that the catalytic activities of CAT on hydrogen peroxide were directly inhibited by N-GQDs, implying that the valence stage change of iron ions (Fe (III)-E→ Fe (IV)-E (.+)→ Fe (III)-E) was heavily disrupted by N-GQDs. We also discovered that CAT activities and mRNA expression levels of *cat* were restrained in N-GQDs exposed zebrafish. Similarly, CAT, SOD, Hb, MPO, and the mitochondrial redox carriers (complex I, complex II, and complex IV) were significantly inhibited by GQDs in term of their enzyme activities or transcription levels. Generally, these antioxidant enzymes depressed by N-GQDs are basically the members of hemoprotein superfamily (Heme Protein Database: http://hemeprotein.info/heme.php). Hemoproteins are a large class of metalloproteins, which contain a heme prosthetic group and are chemically structured by an 'irons cation' encompassed by 'porphyrin bases'. Thus, the antioxidant activities of hemoproteins are greatly determined by the oxidation state of iron ion [76]. Accordingly, we identified the high expression level of transferrin a, which is associated with the total iron binding capacity in blood plasma [77]. It can be deduced that the free iron ions released from TFA decreased, and then likely caused adverse effects to the synthesis of red blood cells. The high levels of TFA are usually the risk index for hypoferric anemia, acute viral hepatitis, and hepatic necrosis [78]. However, some antioxidant enzymes, such as GPx and CYP1A, are highly activated by N-GQDs. GPx is a selenium-containing enzyme, which is responsible for the reduction of lipid hydroperoxides and hydrogen peroxide [59]. Like GO and CNTs, N-GQDs can promote *in vivo* GPx activities, suggesting that the charge-transfer state of GSH→ GS-SG induced by N-GQDs was different from those iron-containing peroxidases, and the underlying biochemical mechanisms remain to be investigated in the future. P450 monooxygenases are also the members of the hemoprotein superfamily, whose main role is to metabolize various physiologic and xenobiotic organic compounds [79]. It is well known that GQDs share the aromatic structure with G and GO. Our study showed that both N-GQDs and USGO can induce high expression levels of *cyp1a*, suggesting that these NPs were effectively metabolized by P450 monooxygenases *via* the canonical AhR signaling pathway, which was shown in the previous studies [10,80]. Furthermore, the activation of *ahrr1* and *ahhr2* implied that NPs can directly act as the mimic ligands to bind with aryl hydrocarbon receptor (AhR) and accelerate the expression levels of P450 monooxygenases (Fig. 9).

5. Conclusion

Our results provide preliminary evidence of the potential adverse effects of N-GQDs *in vivo* system. Although derived from GO, N-GQDs do not inherit most toxicity mechanisms from its parent and develop specific biological effects using *in vivo* system. We here reported the fluorescence enhancement effects and bio-accumulative effects of N-GQDs in zebrafish models, and revealed that N-GQDs could perturb the endogenous antioxidant enzyme system *via* transcriptional or post-transcriptional repression of antioxidant enzymes. Since the antioxidant enzyme system is the key complex underlying the natural immune system to resist dangerous xenotics, it should be careful about the disturbing effects of nanoparticles on organisms. Thus, a better understanding of the molecular mechanism of various types of GQDs can contribute to developing more biocompatible GQDs for biomedical uses in the future.

Conflicts of interest

The authors declare no conflict of interest.

Acknowledgments

The authors are grateful for the supports from the CAS Team Project of the Belt and Road (to D.S.P.) and the Three Hundred Leading Talents

in Scientific and Technological Innovation Program of Chongqing (No. CSTCCXLJRC201714).

Appendix A. Supplementary data

Supplementary data to this article can be found online at https://doi.org/10.1016/j.biomaterials.2019.03.028.

References

[1] M. Bacon, S.J. Bradley, T. Nann, Graphene quantum dots, Part. Part. Syst. Char. 31 (2014) 415–428.
[2] K.A. Ritter, J.W. Lyding, The influence of edge structure on the electronic properties of graphene quantum dots and nanoribbons, Nat. Mater. 8 (2009) 235–242.
[3] L. Li, G. Wu, G. Yang, J. Peng, J. Zhao, J.-J. Zhu, Focusing on luminescent graphene quantum dots: current status and future perspectives, Nanoscale 5 (2013) 4015–4039.
[4] C. Ren, X. Hu, Q. Zhou, Graphene oxide quantum dots reduce oxidative stress and inhibit neurotoxicity in vitro and in vivo through catalase-like activity and metabolic regulation, Adv. Sci. 5 (2018) 1700595.
[5] X.T. Zheng, A. Ananthanarayanan, K.Q. Luo, P. Chen, Glowing graphene quantum dots and carbon dots: properties, syntheses, and biological applications, Small 11 (2015) 1620–1636.
[6] J. Shen, Y. Zhu, X. Yang, C. Li, Graphene quantum dots: emergent nanolights for bioimaging, sensors, catalysis and photovoltaic devices, Chem. Commun. 48 (2012) 3686–3699.
[7] Z.L. Wu, M.X. Gao, T.T. Wang, X.Y. Wan, L.L. Zheng, C.Z. Huang, A general quantitative pH sensor developed with dicyandiamide N-doped high quantum yield graphene quantum dots, Nanoscale 6 (2014) 3868–3874.
[8] J. Sun, S. Yang, Z. Wang, H. Shen, T. Xu, L. Sun, et al., Ultra-high quantum yield of graphene quantum dots: aromatic-nitrogen doping and photoluminescence mechanism, Part. Part. Syst. Char. 32 (2015) 434–440.
[9] D. Qu, M. Zheng, L. Zhang, H. Zhao, Z. Xie, X. Jing, et al., Formation mechanism and optimization of highly luminescent N-doped graphene quantum dots, Sci. Rep. 4 (2014) 5294.
[10] J.-H. Zhang, T. Sun, A. Niu, Y.-M. Tang, S. Deng, W. Luo, et al., Perturbation effect of reduced graphene oxide quantum dots (rGOQDs) on aryl hydrocarbon receptor (AhR) pathway in zebrafish, Biomaterials 133 (2017) 49–59.
[11] G. Qu, S. Liu, S. Zhang, L. Wang, X. Wang, B. Sun, et al., Graphene oxide induces toll-like receptor 4 (tlr4)-dependent necrosis in macrophages, ACS Nano 7 (2013) 5732–5745.
[12] Y. Zhao, Q. Wu, D. Wang, A microRNAs-mRNAs network involved in the control of graphene oxide toxicity in Caenorhabditis elegans, RSC Adv. 5 (2015) 92394–92405.
[13] M. Xu, J. Zhu, F. Wang, Y. Xiong, Y. Wu, Q. Wang, et al., Improved in vitro and in vivo biocompatibility of graphene oxide through surface modification: poly(acrylic acid)-functionalization is superior to pegylation, ACS Nano 10 (2016) 3267–3281.
[14] J. Zhu, M. Xu, M. Gao, Z. Zhang, Y. Xu, T. Xia, et al., Graphene oxide induced perturbation to plasma membrane and cytoskeletal meshwork sensitize cancer cells to chemotherapeutic agents, ACS Nano 11 (2017) 2637–2651.
[15] S. Zhu, J. Zhang, C. Qiao, S. Tang, Y. Li, W. Yuan, et al., Strongly green-photoluminescent graphene quantum dots for bioimaging applications, Chem. Commun. 47 (2011) 6858–6860.
[16] S. Zhu, J. Zhang, S. Tang, C. Qiao, L. Wang, H. Wang, et al., Surface chemistry routes to modulate the photoluminescence of graphene quantum dots: from fluorescence mechanism to up-conversion bioimaging applications, Adv. Funct. Mater. 22 (2012) 4732–4740.
[17] J. Peng, W. Gao, B.K. Gupta, Z. Liu, R. Romero-Aburto, L. Ge, et al., Graphene quantum dots derived from carbon fibers, Nano Lett. 12 (2012) 844–849.
[18] M. Zhang, L. Bai, W. Shang, W. Xie, H. Ma, Y. Fu, et al., Facile synthesis of water-soluble, highly fluorescent graphene quantum dots as a robust biological label for stem cells, J. Mater. Chem. 22 (2012) 7461–7467.
[19] L. Zhang, Y. Xing, N. He, Y. Zhang, Z. Lu, J. Zhang, et al., Preparation of graphene quantum dots for bioimaging application, J. Nanosci. Nanotechnol. 12 (2012) 2924–2928.
[20] D. Jiang, Y. Chen, N. Li, W. Li, Z. Wang, J. Zhu, et al., Synthesis of luminescent graphene quantum dots with high quantum yield and their toxicity study, PLoS One 10 (2016) e0144906.
[21] R.V. Goreham, K.L. Schroeder, A. Holmes, S.J. Bradley, T. Nann, Demonstration of the lack of cytotoxicity of unmodified and folic acid modified graphene oxide quantum dots, and their application to fluorescence lifetime imaging of HaCaT cells, Microchim. Acta 185 (2018) 128.
[22] Y. Chong, Y.F. Ma, H. Shen, X.L. Tu, X. Zhou, J.Y. Xu, et al., The in vitro and in vivo toxicity of graphene quantum dots, Biomaterials 35 (2014) 5041–5048.
[23] Y.-J. Dai, Y.-F. Jia, N. Chen, W.-P. Bian, Q.-K. Li, Y.-B. Ma, et al., Zebrafish as a model system to study toxicology, Environ. Toxicol. Chem. 33 (2014) 11–17.
[24] K. Dooley, L.I. Zon, Zebrafish: a model system for the study of human disease, Curr. Opin. Genet. Dev. 10 (2000) 252–256.
[25] N.D. Lawson, B.M. Weinstein, Arteries and veins: making a difference with zebrafish, Nat. Rev. Genet. 3 (2002) 674–682.
[26] J. Cheng, E. Flahaut, S.H. Cheng, Effect of carbon nanotubes on developing zebrafish (Danio Rerio) embryos, Environ. Toxicol. Chem. 26 (2007) 708–716.
[27] X.T. Liu, X.Y. Mu, X.L. Wu, L.X. Meng, W.B. Guan, Y.Q. Ma, et al., Toxicity of multi-walled carbon nanotubes, graphene oxide, and reduced graphene oxide to zebrafish embryos, Biomed. Environ. Sci. 27 (2014) 676–683.
[28] Y. Chen, X. Hu, J. Sun, Q. Zhou, Specific nanotoxicity of graphene oxide during zebrafish embryogenesis, Nanotoxicology 10 (2016) 42–52.
[29] T.C. King-Heiden, P.N. Wiecinski, A.N. Mangham, K.M. Metz, D. Nesbit, J.A. Pedersen, et al., Quantum dot nanotoxicity assessment using the zebrafish embryo, Environ. Sci. Technol. 43 (2009) 1605–1611.
[30] W. Zhang, X. Sun, L. Chen, K.-F. Lin, Q.-X. Dong, C.-J. Huang, et al., Toxicological effect of joint cadmium selenium quantum dots and copper ion exposure on zebrafish, Environ. Toxicol. Chem. 31 (2012) 2117–2123.
[31] S. Tang, Q. Cai, H. Chibli, V. Allagadda, J.L. Nadeau, G.D. Mayer, Cadmium sulfate and CdTe-quantum dots alter DNA repair in zebrafish (Danio rerio) liver cells, Toxicol. Appl. Pharmacol. 272 (2013) 443–452.
[32] P.N. Wiecinski, K.M. Metz, T.C. King Heiden, K.M. Louis, A.N. Mangham, R.J. Hamers, et al., Toxicity of oxidatively degraded quantum dots to developing zebrafish (danio rerio), Environ. Sci. Technol. 47 (2013) 9132–9139.
[33] Z.G. Wang, R. Zhou, D. Jiang, J.E. Song, Q. Xu, J. Si, et al., Toxicity of graphene quantum dots in zebrafish embryo, Biomed. Environ. Sci. 28 (2015) 341–351.
[34] H. Zhang, C. Peng, J. Yang, M. Lv, R. Liu, D. He, et al., Uniform ultrasmall graphene oxide nanosheets with low cytotoxicity and high cellular uptake, ACS Appl. Mater. Interfaces 5 (2013) 1761–1767.
[35] M.S.U. Rehman, N. Rashid, M. Ashfaq, A. Saif, N. Ahmad, J.-I. Han, Global risk of pharmaceutical contamination from highly populated developing countries, Chemosphere 138 (2015) 1045–1055.
[36] J. Modrzynska, T. Berthing, G. Ravn-Haren, N.R. Jacobsen, I.K. Weydahl, K. Loeschner, et al., Primary genotoxicity in the liver following pulmonary exposure to carbon black nanoparticles in mice, Part. Fibre Toxicol. 15 (2018) 2.
[37] T. Kosmehl, A.V. Hallare, G. Reifferscheid, W. Manz, T. Braunbeck, H. Hollert, A novel contact assay for testing genotoxicity of chemicals and whole sediments in zebrafish embryos, Environ. Toxicol. Chem. 25 (2006) 2097–2106.
[38] X. Zhu, J. Wang, X. Zhang, Y. Chang, Y. Chen, The impact of ZnO nanoparticle aggregates on the embryonic development of zebrafish (Danio rerio), Nanotechnology 20 (2009) 195103.
[39] Y.-B. Ma, C.-J. Lu, M. Junaid, P.-P. Jia, L. Yang, J.-H. Zhang, et al., Potential adverse outcome pathway (AOP) of silver nanoparticles mediated reproductive toxicity in zebrafish, Chemosphere 207 (2018) 320–328.
[40] C. Ren, X. Hu, Q. Zhou, Graphene oxide quantum dots reduce oxidative stress and inhibit neurotoxicity in vitro and in vivo through catalase-like activity and metabolic regulation, Adv. Sci. 5 (2018) 1700595.
[41] G.J. Lieschke, A.C. Oates, M.O. Crowhurst, A.C. Ward, J.E. Layton, Morphologic and functional characterization of granulocytes and macrophages in embryonic and adult zebrafish, Blood 98 (2001) 3087.
[42] M. Furutani-Seiki, Y.J. Jiang, M. Brand, C.P. Heisenberg, C. Houart, D. Beuchle, et al., Neural degeneration mutants in the zebrafish, Danio rerio, Development 123 (1996) 229.
[43] M.E. Robu, J.D. Larson, A. Nasevicius, S. Beiraghi, C. Brenner, S.A. Farber, et al., p53 activation by knockdown technologies, PLoS Genet. 3 (2007) e78.
[44] R. Pamanji, B. Yashwanth, J. Venkateswara Rao, Profenofos induced biochemical alterations and in silico modelling of hatching enzyme, ZHE1 in zebrafish (Danio rerio) embryos, Environ. Toxicol. Pharmacol. 45 (2016) 123–131.
[45] Holtzinger A, Evans T. Gata 4 Regulates the Formation of Multiple Organs.
[46] S.-L. Xie, M. Junaid, W.-P. Bian, J.-J. Luo, J.H. Syed, C. Wang, et al., Generation and application of a novel transgenic zebrafish line Tg(cyp1a:mCherry) as an in vivo assay to sensitively monitor PAHs and TCDD in the environment, J. Hazard Mater. 344 (2018) 723–732.
[47] J.A. Horsfield, S.H. Anagnostou, J.K.-H. Hu, K.H.Y. Cho, R. Geisler, G. Lieschke, et al., Cohesin-dependent regulation of Runx genes, Development 134 (2007) 2639.
[48] Y. Liu, M. Junaid, Y. Wang, Y.-M. Tang, W.-P. Bian, W.-X. Xiong, et al., New toxicogenetic insights and ranking of the selected pharmaceuticals belong to the three different classes: a toxicity estimation to confirmation approach, Aquat. Toxicol. 201 (2018) 151–161.
[49] M.M. Bradford, A rapid and sensitive method for the quantitation of microgram quantities of protein utilizing the principle of protein-dye binding, Anal. Biochem. 72 (1976) 248–254.
[50] A.T. McCurley, G.V. Callard, Characterization of housekeeping genes in zebrafish: male-female differences and effects of tissue type, developmental stage and chemical treatment, BMC Mol. Biol. 9 (2008) 102.
[51] R.E. Weber, F.B. Jensen, Functional adaptations in hemoglobins from ectothermic vertebrates, Annu. Rev. Physiol. 50 (1988) 161–179.
[52] C.C.W. Hsia, Respiratory function of hemoglobin, N. Engl. J. Med. 338 (1998) 239–248.
[53] B.J. Reeder, Redox and peroxidase activities of the hemoglobin superfamily: relevance to health and disease, Antioxidants Redox Signal. 26 (2016) 763–776.
[54] Y. Li, Y. Zhao, H. Cheng, Y. Hu, G. Shi, L. Dai, et al., Nitrogen-doped graphene quantum dots with oxygen-rich functional groups, J. Am. Chem. Soc. 134 (2012) 15–18.
[55] L. Lin, X. Song, Y. Chen, M. Rong, T. Zhao, Y. Wang, et al., Intrinsic peroxidase-like catalytic activity of nitrogen-doped graphene quantum dots and their application in the colorimetric detection of H_2O_2 and glucose, Anal. Chim. Acta 869 (2015) 89–95.
[56] M. Nurunnabi, Z. Khatun, K.M. Huh, S.Y. Park, D.Y. Lee, K.J. Cho, et al., In vivo biodistribution and toxicology of carboxylated graphene quantum dots, ACS Nano 7 (2013) 6858–6867.
[57] P. Chelikani, I. Fita, P.C. Loewen, Diversity of structures and properties among catalases, Cell. Mol. Life Sci. 61 (2004) 192–208.
[58] J.M. McCord, I. Fridovich, Superoxide Dismutase: an enzymic function for erythrocuprein (hemocuprein), J. Biol. Chem. 244 (1969) 6049–6055.

[59] K.P. Bhabak, G. Mugesh, Functional mimics of glutathione peroxidase: bioinspired synthetic antioxidants, Acc. Chem. Res. 43 (2010) 1408–1419.
[60] C. Pretti, M. Oliva, R.D. Pietro, G. Monni, G. Cevasco, F. Chiellini, et al., Ecotoxicity of pristine graphene to marine organisms, Ecotoxicol. Environ. Saf. 101 (2014) 138–145.
[61] X. Hu, K. Lu, L. Mu, J. Kang, Q. Zhou, Interactions between graphene oxide and plant cells: regulation of cell morphology, uptake, organelle damage, oxidative effects and metabolic disorders, Carbon 80 (2014) 665–676.
[62] P. Banerjee, S. Sau, P. Das, A. Mukhopadhayay, Optimization and modelling of synthetic azo dye wastewater treatment using Graphene oxide nanoplatelets: characterization toxicity evaluation and optimization using Artificial Neural Network, Ecotoxicol. Environ. Saf. 119 (2015) 47–57.
[63] K.A. Patlolla, J. Randolph, A.S. Kumari, B.P. Tchounwou, Toxicity evaluation of graphene oxide in kidneys of sprague-dawley rats, Int. J. Environ. Res. Public Health 13 (2016).
[64] M. Dziewięcka, J. Karpeta-Kaczmarek, M. Augustyniak, Majchrzycki Ł, M.A. Augustyniak-Jabłokow, Evaluation of in vivo graphene oxide toxicity for Acheta domesticus in relation to nanomaterial purity and time passed from the exposure, J. Hazard Mater. 305 (2016) 30–40.
[65] S. Huang, H. Qiu, S. Lu, F. Zhu, Q. Xiao, Study on the molecular interaction of graphene quantum dots with human serum albumin: combined spectroscopic and electrochemical approaches, J. Hazard Mater. 285 (2015) 18–26.
[66] M. Chen, J. Yin, Y. Liang, S. Yuan, F. Wang, M. Song, et al., Oxidative stress and immunotoxicity induced by graphene oxide in zebrafish, Aquat. Toxicol. 174 (2016) 54–60.
[67] S. Zhu, F. Luo, W. Chen, B. Zhu, G. Wang, Toxicity evaluation of graphene oxide on cysts and three larval stages of Artemia salina, Sci. Total Environ. 595 (2017) 101–109.
[68] Z. Wang, F. Zhang, S. Wang, W.J.G.M. Peijnenburg, Assessment and prediction of joint algal toxicity of binary mixtures of graphene and ionic liquids, Chemosphere 185 (2017) 681–689.
[69] B. Zhu, S. Zhu, J. Li, X. Hui, G.-X. Wang, The developmental toxicity, bioaccumulation and distribution of oxidized single walled carbon nanotubes in Artemia salina, Toxicol. Res. 7 (5) (2018) 897–906.
[70] K. Srikanth, L.S. Sundar, E. Pereira, C. Duarte Armando, Graphene oxide induces cytotoxicity and oxidative stress in bluegill sunfish cells, J. Appl. Toxicol. 38 (2017) 504–513.
[71] Y. Chong, C. Ge, G. Fang, X. Tian, X. Ma, T. Wen, et al., Crossover between anti- and pro-oxidant activities of graphene quantum dots in the absence or presence of light, ACS Nano 10 (2016) 8690–8699.
[72] P. Han, X.-H. Zhou, N. Chang, C.-L. Xiao, S. Yan, H. Ren, et al., Hydrogen peroxide primes heart regeneration with a derepression mechanism, Cell Res. 24 (2014) 1091.
[73] C. Gauron, F. Meda, E. Dupont, S. Albadri, N. Quenech'Du, E. Ipendey, et al., Hydrogen peroxide (H2O2) controls axon pathfinding during zebrafish development, Dev. Biol. 414 (2016) 133–141.
[74] R.K. Banerjee, Nonsteroidal anti-inflammatory drugs inhibit gastric peroxidase activity, Biochim. Biophys. Acta Gen. Subj. 1034 (1990) 275–280.
[75] I. Chattopadhyay, U. Bandyopadhyay, K. Biswas, P. Maity, R.K. Banerjee, Indomethacin inactivates gastric peroxidase to induce reactive-oxygen-mediated gastric mucosal injury and curcumin protects it by preventing peroxidase inactivation and scavenging reactive oxygen, Free Radic. Biol. Med. 40 (2006) 1397–1408.
[76] P.R.O. Montellano, Catalytic sites of hemoprotein peroxidases, Annu. Rev. Pharmacol. Toxicol. 32 (1992) 89–107.
[77] C.R. R, C.-W. Mireille, Iron transport and storage, Eur. J. Biochem. 164 (1987) 485–506.
[78] Brugnara C. Iron Deficiency and Erythropoiesis: New Diagnostic Approaches 2003.
[79] F. Hannemann, A. Bichet, K.M. Ewen, R. Bernhardt, Cytochrome P450 systems-biological variations of electron transport chains, Biochim. Biophys. Acta Gen. Subj. 1770 (2007) 330–344.
[80] S. Deng, P.-P. Jia, J.-H. Zhang, M. Junaid, A. Niu, Y.-B. Ma, et al., Transcriptomic response and perturbation of toxicity pathways in zebrafish larvae after exposure to graphene quantum dots (GQDs), J. Hazard Mater. 357 (2018) 146–158.